Available online at www.sciencedirect.com
ScienceDirect
Journal of Photochemistry and Photobiology A: Chemistry 189 (2007) 80–85
Journal of Photochemistry and Photobiology A:Chemistry
www.elsevier.com/locate/jphotochem

Study of photocatalytic oxidation of indigo carmine dye on Mn-supported TiO_2

I. Othman [a,*], R.M. Mohamed [b], F.M. Ibrahem [c]

[a] *Faculty of Science, Chemistry Department, Al-Azhar University, Naser City, Cairo, Egypt*
[b] *Central Metallurgical R&D Institute, Department of Nanostructured Material, Helwan, Cairo, Egypt*
[c] *Faculty of Science, Chemistry Department, Suez Canal University, Ismailia, Egypt*

Received 4 November 2006; received in revised form 7 January 2007; accepted 12 January 2007
Available online 17 January 2007

Abstract

A detailed comparative investigation on the discoloration (adsorption) and mineralization (in the presence of UV irradiation) of indigo carmine (IC) dye over four photocatalysts TiO_2-D (from Degussa), TiO_2-SG (prepared with a sol–gel method), Mn/TiO_2-imp (prepared with an impregnation method) and Mn/TiO_2-SG (prepared with a sol–gel method) is presented. The experimental results show that Mn/TiO_2-imp gives the highest photocatalytic activity. Whoever, the influence of pH, catalyst amount and time on the decolorization rate of IC on Mn/TiO_2-imp was thoroughly discussed and correlated with ZPC of MnO_x species, various exposed species of MnO_x and surface properties. XRD, FT-IR and N_2 adsorption measurements were used as characterization techniques over the calcined catalysts at 550 °C. Electric conductivity measurements by applying zeta potential technique provide an insight into the electric static situation of the particles at a given pH.

Keywords: Dye decolorization; Mn/TiO_2; Titania; Manganese; Sol–gel texturing; XRD; N_2 adsorption

1. Introduction

Indigo carmine (IC) is one of the oldest dyes and still one of the most important used. Its major industrial application is the dyeing of clothes (blue jeans) and other blue denim [1]. Indigo carmine is also used for medical diagnostic purposes, in conjunction with acetic acid the dye facilitate diagnosis of Barrett's esophagus [2]. It can also help to target biopsies even better, since in homogeneously stained or unstained areas seem to correlate with intraepithelial neoplasia [3]. Indigo carmine, however, is not readily metabolized but is rather freely filterable by the kidneys, giving intravenous injection of indigo carmine for intra-operative cystoscopy is a safe technique that can detect otherwise undetected intra-operative compromise of the urinary tract [4].

The dye indigo carmine is considered a highly toxic indigoid class of dye and its touch can cause skin and eye irritations to human being. It can also cause permanent injury to cornea and conjunctiva. The consumption of the dye can also prove fatal, as it is carcinogenic in nature and can lead to reproductive, developmental, neuro and acute toxicity [5]. It has also been established that the dye leads to tumors at the site of application [6]. When administered intravenously to determine potency of the urinary collecting system, it has also been reported to cause mild to severe hypertension, cardiovascular and respiratory effects in patients [7]. It may also cause gastrointestinal irritation with nausea, vomiting and diarrhea [8].

Thus, keeping the toxicity of this dye in view, various attempts have been made for the removal of indigo carmine from water and wastewater [9–12].

Doping titania with transition metal ions has been tested as a promising way of improving the photocatalytic activity of semiconductor oxides. The incorporation of metal ions into titania crystal lattice can significantly extend the absorption by the photocatalysts into visible range. The effect of doping is to change the equilibrium concentration of electrons or holes [13–15].

Previous studies on the phase transformation characteristics of doped TiO_2 have shown stabilization of both anatase and rutile phases for different experimental conditions. For examples, the work of Arroyo et al. [16] on manganese (Mn^{2+}) doped titania

* Corresponding author. Tel.: +20 125169213.
E-mail address: iothmana@yahoo.com (I. Othman).

1010-6030/$ – see front matter © 2007 Elsevier B.V. All rights reserved.
doi:10.1016/j.jphotochem.2007.01.010

showed stabilization of the anatase phase for low doping levels, prior to segregation of the doping to the surface at higher concentration and stabilization of the rutile phase.

MnO_2 was among the oldest examined metal oxide catalyst and found to possess a potential activity in redox reaction. Unfortunately, it has been shown that manganese oxides are insoluble [17,18]. However, the amount of manganese dissolved in solution can be increased considerably in acidic medium with the addition of organic compounds such as dyes [19]. But the further adsorption and oxidation of dye compound on the mineral particles interface reduce their surface areas and lead to inhibition of the process [20]. In this paper, we have studied the preparation of Mn on titania by different methods and characterized by X-ray diffraction, FT-IR, particle size distribution, N_2 adsorption and electrical conductivity. Finally, the decolorization of indigo carmine (IC) in the absence and presence of UV lamp is investigated for all samples.

2. Experimental

2.1. Materials

Titanium dioxide powder P-25 (TiO_2-D) is predominantly anatase it was purchased from Degussa (Germany) and was used without any further treatment. Manganese nitrate [$Mn(NO_3)_2$] (Merck), titanium(IV) isobutoxide [Fluka], ethanol and deionized water.

Indigo carmine dye [3,3′-dioxo-1,3,1′,3′-tetrahydro-[2,2′]-bi-indolylidene-5,5′-disulfonic acid disodium salt] was delivered from the General Chemical Co. Ltd., Wembley Middlesex, England.

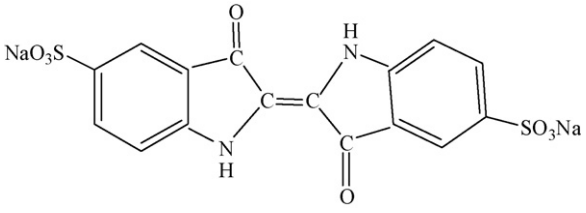

MF $C_{16}H_8N_2Na_2O_8S_2$, MW 466.35 g/L. The peak intensity is at 608 nm; molar absorbtivity is 6309 mol^{-1} cm^{-1}.

2.1.1. Preparation of TiO_2 by sol–gel

Titania sol–gel was synthesized exhibiting the molar ratio:$Ti(C_4H_9O_4)$:20 C_2H_5OH:4H_2O:0.001 HNO_3

In each case, $Ti(C_4H_9O_4)$ was first dissolved in ethanol medium forming a solution, water and nitric acid added dropwise into the formed sol with a stirring for about 30 min at room temperature. The prepared sol was left to stand for the formation of gel. After the gelation was completed, the gels were aged for 24 h at room temperature and then calcined at 550 °C for 5 h. This sample was referred to TiO_2-SG.

2.1.2. Preparation of Mn/TiO_2 by impregnation

Manganese oxide on TiO_2-D prepared using an aqueous solution of $Mn(NO_3)_2$. The used amount of solution was necessary to complete wetness of the sample.

The reaction temperature was adapted at 80 °C for 4 h using temperature controller type (REX-P 90). The precursor sample was then dried at 110 °C overnight and calcined in air at 550 °C for 6 h. This sample was referred to Mn–TiO_2-imp.

2.1.3. Preparation of Mn/TiO_2 by sol–gel

Manganese loaded on TiO_2-D prepared by adding $Mn(NO_3)_2$ solution to Ti(IV) isobutoxide at constant temperature 60 °C using a water/solvent ratio of 4:1. The solids were dried at 120 °C for 12 h and calcined in air at 550 °C for 4 h. Mn loading was 10 wt.% in all the prepared samples. This sample was referred to Mn–TiO_2-SG.

2.2. Characterization techniques

2.2.1. X-ray diffraction analysis (XRD)

The X-ray diffraction patterns for various titania samples were obtained using a Bruker axs, D8 advance. Ni-filtered copper radiation ($\lambda = 1.5404$ Å). Bruker generator operating at 30 kV and 10 mA. Spectra was scanned at a rate of 2.5 ° min^{-1} in a 2θ. The phases of TiO_2 and MnO_2 have been identified by comparison with GCPDS database. The results were presented as continues traces of intensity as a function of 2θ.

2.2.2. FT-IR absorption analysis

FT-IR spectra were performed using Jasco FT-IR-460 plus, Japan spectrophotometer, over the range of frequencies from 3800 to 3300 and 1000 to 450 cm^{-1} with a resolution of 2 cm^{-1} adapting the technique of KBr pellets.

2.2.3. Surface area measurement

The nitrogen adsorption isotherms were measured at −196 °C using a conventional volumetric apparatus. The specific surface area was obtained using the BET method.

2.2.4. Zeta potential measurements

Zeta potentials of suspension samples were measured at room temperature using a zeta meter 3.0 equipped with a microprocessor unit. The unit automatically calculates the electrophoretic mobility of the particle and converting it into zeta potential using Smoluchowski equation. A 0.1 g amount of the solid sample was dissolved in 50 ml of 0.001 M NaCl solutions at various pH values for 24 h in a shaking bath. Before measuring, the suspension was kept for 5 min settling the large particles. Each data point is an average of approximately 20 measurements. The pH of the suspension was adjusted using dilute HCl and NaOH [17]. All solutions were prepared using bidistilled water. The pH of the suspension was measured using a pH meter (Orion 920A).

2.3. Investigation of the catalytic activity of the prepared catalyst

2.3.1. IC dye adsorption

Adsorption experiments of IC on the prepared catalysts in the absence of ultraviolet irradiation were carried out in a batch mode. A 250 ml of the IC dye (100 ppm), previously adjusted to the required pH value with diluted NaOH and HCl solutions,

was added to a 300 ml beaker containing different amounts of suspended catalysts. The suspensions were immediately shaken in an air for 1 h using a magnetic stirrer. Then fellow up the uptaken amounts of the dye by catalysts that maintained for 1 h adsorption time.

2.3.2. Photocatalytic evaluation

All the experiments were carried out using a horizontal cylinder annular batch reactor. IC was selected, as a model for the photocatalytic degradation experiments because it is a non-volatile and common contaminant in the industrial wastewaters. A black light-blue florescent bulb (F18W-BLB) was located at the axis of the reactor to supply UV illumination. The light intensity after passing through a reaction suspension was 365 nm. The experiments were performed by suspending calculated amount of the catalyst into IC solution (100 ppm). The reaction was carried out isothermally at 25 °C and samples of the reaction mixture were taken at time intervals for a total reaction time 1 h. The disappearance of IC was analyzed by UV–vis spectrophotometer (JASCO V-570 unit, serial no. 29635) over the 190–800 nm range. Calibration plots based on Beer–Lamberts law were established relating the absorbance to the concentration. The decolorization was determined at the maximum 608 nm. Removal efficiency (%) of IC was measured by applying the following equation:

$$\text{removal efficiency}\,(\%) = \frac{C_o - C}{C_o} \times 100$$

where C_o is the original indigo carmine (IC) content and C is the retained IC in solution.

3. Result and discussion

3.1. XRD

XRD results in the form of diffraction patterns (intensity versus 2θ), the figure are not given here. Inspection of the obtained XRD patterns and the relevant phase changes would reveal the following:

- TiO_2 (anatase phase), as a major phase dominated the bulk composition of the TiO_2-D and Mn/TiO_2-imp, whereas the system TiO_2-SG and Mn/TiO_2-SG showed the characteristic diffraction lines of TiO_2 (anatase) beside TiO_2 (rutile).
- Having examined the respective data, one could observe that the inclusion of Mn in the matrix of supported system give rise to measurable diminishing in the degree of crystallinity and crystal size of the presented phases.
- It is worth noting that, diffraction peak of Mn is undetectable in the diffractograms of Mn containing solids, this could attributed to the high degree of dispersion of Mn species and/or the incorporation of Mn ions in the matrix of TiO_2-support material forming solid solution.
- There is no relation between the close similarity of the ionic radii between Mn^{3+} (0.66 Å) and Ti^{4+} (0.68 Å) and the change of lattice parameter of TiO_2 lattice. Indeed, this anticipation has been confirmed experimentally.

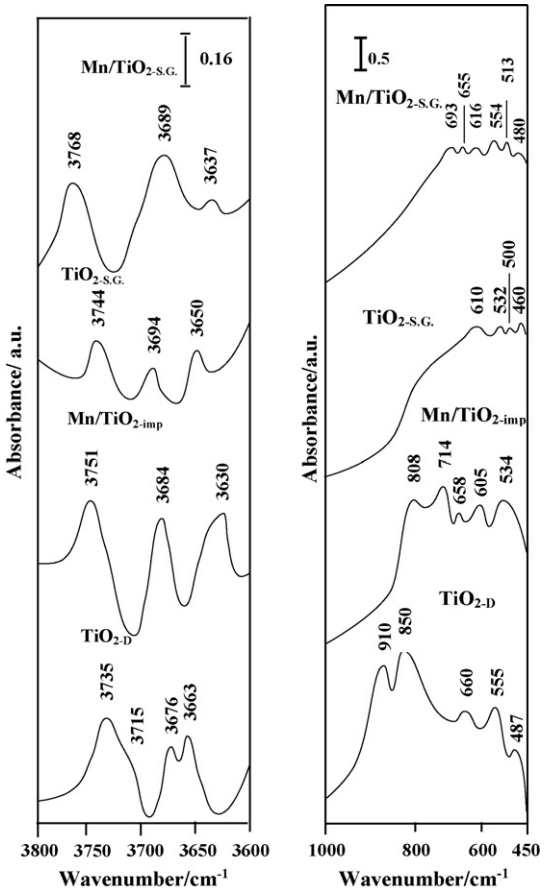

Fig. 1. FT-IR spectra of TiO_2-D, Mn/TiO_2-imp, TiO_2-SG, and Mn/TiO_2-SG in the low frequency region (450–1300 cm^{-1}) and high OH groups region (3600–4000 cm^{-1}).

3.2. FT-IR absorption analysis

The FT-IR spectra of the investigated TiO_2-D, Mn/TiO_2-D, TiO_2-SG and Mn/TiO_2-SG samples are illustrated in Fig. 1. The spectra of Fig. 1 point out the following:

- The spectrum of TiO_2-D displays strong absorption bands at 487 and 555 cm^{-1} which are due to the vibration of the Ti–O bond in the TiO_2 lattice [22,23].
- The peaks centered at 850–910 cm^{-1} may be assigned to stretching vibration of O–O for peroxo groups, thus the shoulder observed at 660 cm^{-1} may have been due to the vibration of the Ti–O–O bond [23].
- The spectrum of Mn/TiO_2-imp shows the appearance of new band at 605 cm^{-1} that was absent in the parent TiO_2-D sample thus, it is reasonable to associate it with Mn–O vibrations and more specifically to lattice vibrations of M^{III}–O bonds [24–27].
- Moreover, there is a shift observed of the following bands to lower wavelength value 555–535 and 850–808 cm^{-1}, in addition to disappearance of the band located at 910 cm^{-1}, indeed that is related to the interaction between Mn and Ti.
- The spectrum of TiO_2-SG shows that bands characterized by anatase (three bands at 532 and 610 cm^{-1}) and rutile (one

band at 460 cm^{-1}), which can be assigned to vibration modes of titanium oxide structure, O–Ti–O [23].

- Examining spectra of TiO_2-SG and Mn/TiO_2-SG, revealed bands at 610, 532, 500 and 460 cm^{-1} shifted absorption to 616, 554, 513 and 480 in Mn/TiO_2-SG due to the interaction association between Mn and Ti. New band at 655 and 693 cm^{-1} could be attributed vibration modes of β-MnO_2 which assumes a tetragonal structure [24,28].
- The IR spectrum of OH groups in the parent TiO_2-D shows bands at 3736, 3715, 3676 and 3663 cm^{-1} (Fig. 1, these peaks were assigned to isolated surface hydroxyl groups [29,30]).
- It is worth mentioning that, Mn incorporation cause increase of the band intensity of the free OH groups of TiO_2-D with a marked increase in wave numbers 3736 (to 3752 cm^{-1}) together with vanishing those at 3715 and 3676 cm^{-1}. Simultaneously, new band at 3630 cm^{-1} appear in Mn/TiO_2-imp. The former band is indicative for OH groups at Mn atoms on non-framework positions and represents acidic hydroxyls of varied strength.
- However, the OH groups in TiO_2 prepared by sol–gel technique appeared 3744, 3694 and 3650 cm^{-1} these bands related to free hydroxyl groups. The band at 3744 shifted to the higher at (3768 cm^{-1}) when introduced Mn by sol–gel. The observed shift of the OH stretch from 3744 to 3768 cm^{-1} upon introduction of Mn signals a decrease, not an increase in the acidity of the proton; Brønsted acidity is well known to be accompanied by a red shift of the OH stretch This difference shows that the force constant of the O–H bond is greater for Mn than TiO_2 and this fact implies that the hydroxylic hydrogen atom is more protonic for the former than for the latter [31].

3.3. Surface and texturing characteristic of the investigated catalysts

The different surface characteristics of the investigated solid samples were determined and the data obtained are cited in Table 1. Inspection of this table reveals the following:

- The values of S_{BET} and S_t are similar to each other, indicating the absence of ultra-micropores in the solids investigated.
- A slight decrease in the surface area of TiO_2-D is observed upon the introducing Mn by impregnation method. Generally, this decrease is proportional to the blockage of the titania pores.
- Inclusion of Mn in TiO_2-SG amount increase of 24% S_{BET} this measurable increase could not be attributed to a possible narrowing. Indeed, TiO_2-SG and Mn/TiO_2-SG are close to each other (Table 1). So, one mien think about a possible upward cross in TiO_2 lattice via location of Mn ions in the uppermost surface lyre TiO_2.

Table 1
Textural parameters of various TiO_2 and Mn/TiO_2 materials prepared by different methods

r^- (Å)	V_p (cm^3/g)	S_t (m^2/g)	S_{BET} (m^2/g)	Samples
30	0.334	180	183	TiO_2-D
35	0.320	141	147	Mn/TiO_{2imp}
40	0.361	217	221	TiO_2-SG
39	0.355	268	275	Mn/TiO_2-SG

S_{BET}: surface area derived from BET-method; S_t: surface area derived from *t*-plot method; V_p: pore volume obtained at single point at P/P^0 ~0.95; r^-: pore radius.

3.4. Catalytic activity

3.4.1. Comparison between photocatalysis and decolorization in air

The decolorization efficiency of IC on TiO_2-D, Mn/TiO_2-imp, TiO_2-SG and Mn/TiO_2-SG in the absence or presence of ultraviolet irradiation at pH 2 was shown in Fig. 2. This figure shows a decreasing trend of the catalytic activity in the absence ultraviolet decreased from Mn/TiO_2-imp > Mn/TiO_2-SG > TiO_2-D > TiO_2-SG. In the manganese-supported on titania, either by impregnation or sol–gel methods, the photocatalytic activity is ca. 10 times higher than the values exhibited in absence of UV. As it was explained the additional OH radical, which are powerful oxidants, can non-selectively attack the organic intermediates to complete mineralization. Considerable attention has been paid to, the Mn/TiO_2-SG in which there is only moderate increase in the constant rate, this may be attributed to the insertion of manganese ions in the lattice of TiO_2, increasing the ability of the TiO_2 to produce hole and electrons, which is a very important step in the titania pathway for producing the hydroxyl radicals.

It is obvious in Fig. 2, that the catalytic activity of TiO_2-D higher than TiO_2-SG indicating the high effect of surface hydroxyl population of this sample. This high surface hydroxyl concentration, due to the existence of large extent of the anatase

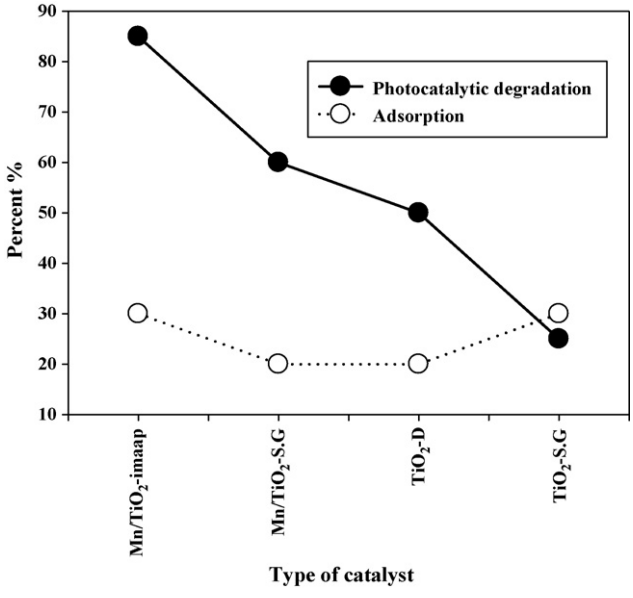

Fig. 2. The efficiency of IC decolorization and photodegradation over various catalysts. Experimental conditions: pH 2, reaction volume 300 ml, catalyst content 100 mg, reaction time 60 min, and initial dye conc. 100 ppm.

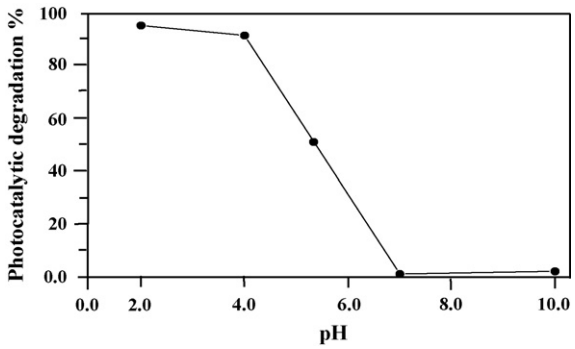

Fig. 3. Effect of pH on the photocatalytic efficiency percentages of IC on Mn/TiO_2-imp. Experimental conditions: reaction volume 300 ml, catalyst content 100 mg, reaction time 60 min, and initial dye conc. 100 ppm.

phase (100%) even though it was calcined at 500 °C, this confirmed by FT-IR analysis.

Enhancing the rate of the reaction of the sample upon exposure to UV irradiation supports that the mechanism is initiated by the HO^* radicals stemming from the Mn^{4+} photoredox directly. The oxidation of the dye on Mn/TiO_2-SG was inactive upon UV irradiation due to the filling of the holes or the reduction–oxidation of Mn^{4+}–Mn^{3+}.

3.4.2. Effect of pH on the photocatalytic efficiency of IC

The photocatalytic efficiency of IC on Mn–TiO_2-imp at different pH values was shown in Fig. 3. The pH of the solution was adjusted with diluted NaOH and HCl. It was found that the photocatalytic efficiency of the dye over MnO_2/TiO_2-imp was highly pH dependent, the photocatalytic efficiencies increased with decreasing pH values. But at pH > 10, the decolorization of the dye was negligible. The photocatalytic efficiency dramatically increased as the pH 2.

The photocatalytic oxidation of organic compounds on manganese oxide may be carried out in two processes:

(1) The diffusion of organic compound to the particle surface to forming a complex.
(2) Exchange of electrons with the reactive surface of MnO_2 [32].

For IC, as a hydrophilic substrate, the diffusion of the neutral species is more easily to it, then accumulate at the surface of MnO_x in comparison with its corresponding ionic forms. The zeta potential profile of the IC/Mn–TiO_2-imp suspension shown in Fig. 4 may further prove the above explanation to some extent. The fluctuation of degradation occurred near pH 4, where is the point of zero charge (PZC) of MnO_2 [33]. Hence, the oxidizing ability of MnO_2 can be sharply enhanced [32]. MnO_x surface is positively charged below pH 4 based on their zpc. IC is a dianionic dye in aqueous solution and it can keep its dianionic configuration in the pH range 3–11. At low pH range, electrostatic interactions between the positive catalyst surface and dye anions lead to strong adsorption of the latter on the metal oxide support.

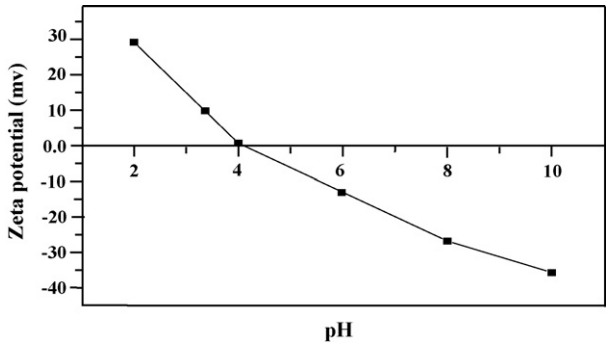

Fig. 4. Zeta potential of IC on Mn/TiO_2-imp as a function of solution pH.

3.4.3. Effect of time on photocatalytic efficiency of IC

It can be seen that the dye uptake process was found to proceed through two stages:

(1) An initial rapid uptake for the first 5 min was found that 40% of IC decolorized as shown in Fig. 5.
(2) The dye uptake attains saturation during 5–40 min and finally increases to reaching 100% degradation in 70 min reaction time. The high value of sorption rate at the initial period (5 min) may be due to increasing the number of vacant sites available at the initial stage and as a result an expected variation in the concentration of adsorbate in solution and on adsorbent surface (concentration gradient) tends to enhance the dye sorption rate. As time proceeds, this concentration gradient decreases due to accumulation of dye molecules on vacant sites and thus saturation stage was almost perceived.

3.4.4. Effect of catalyst loading on photocatalytic efficiency of IC

Experiments were performed to study the variations in the rate of degradation at different catalyst concentration ranging from 0.025 to 0.2 g/dm^3 as shown in Fig. 6. It was observed that the degree of photocatalytic efficiency of IC solution increases with increasing the photocatalyst amount, till 0.1 g. The most

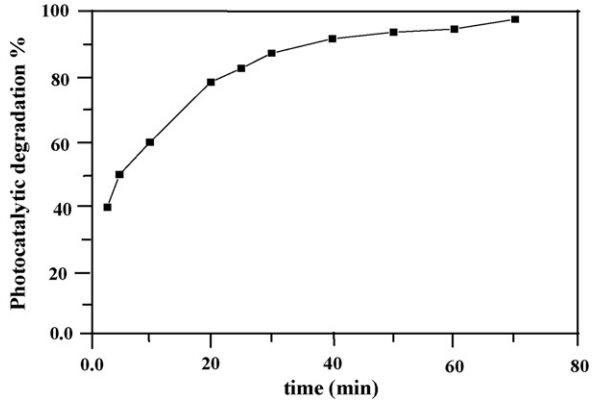

Fig. 5. Kinetics of photocatalytic oxidation of IC on Mn/TiO_2-imp. Experimental condition: pH 2, $T = 25$ °C, catalyst mass = 100 mg, volume = 300 ml, and initial dye conc. 100 ppm.

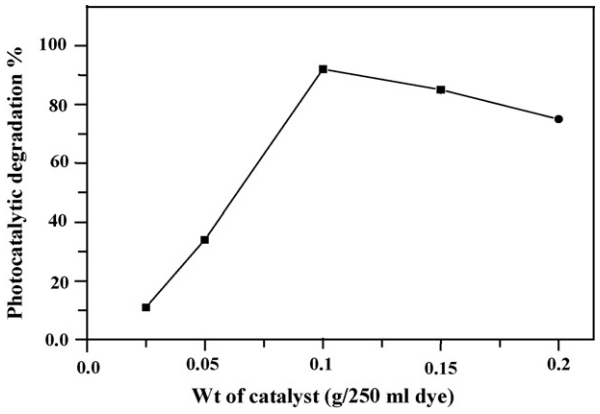

Fig. 6. Effect of photocatalyst content of Mn/TiO_2-imp, on the photocatalytic degradation of IC. Experimental conditions: pH 2, $T = 25\,^{\circ}C$ time = 60 min, volume = 300 ml, and initial dye conc. 100 ppm.

effective decomposition of IC (90%) was observed with the catalyst amount equal to 0.1 g after which (0.15 and 0.2 g of catalyst) the photocatalytic efficiency decreases.

They concluded that the increase of catalyst amounts promote the existence of the presence of parallel paths associated with catalyst degradation during the catalytic cycle (e.g. dimerization reaction) [34], and thus, increases as the concentration of the amount of a catalyst increase. However, attaining complete degradation of the dye at specific catalyst concentration (0.1 g) nullifies the possibility of the presence of competing paths for the reaction and indeed suggests a facile pathway for degradation of such a dye.

4. Conclusion

Studies dealing with manganese-supported titanium synthesized by an impregnation and sol–gel technique showed high photocatalytic and decolorization activities for the removal of IC dye in the sample prepared by impregnation technique. This apparent activity can be explained:

(1) The decreasing of particle size and type of structural Mn comparing with (Mn/TiO_2-imp and Mn/TiO_2-SG).
(2) The presence of acidic hydroxyls specifically those located at $3619\,cm^{-1}$.
(3) The increasing of the pore radius of titanium after Mn incorporation comparing with other prepared samples.
(4) A relative decrease of crystal size of titanium after the incorporation of Mn/TiO_2-imp comparing with Mn/TiO_2-SG.
(5) The reduction–oxidation of Mn^{4+}–Mn^{3+} on the irradiated MnO_x is probably inhibited by introduced Mn inside lattice.

References

[1] F.J. Green (Ed.), The Sigma Aldrich Handbook of Stains, Dyes and Indicators, Aldrich Chemical, Milwaukee, WI, 1990, p. 403.
[2] M. Stolte, M. Vieth, Acta Endosc. 31 (2) (2001) 125.
[3] C.F.I. Jabs, H.P. Drutz, R.L. Summit Jr., Am. J. Obst. Gynecol. 185 (6) (2001) 1368.
[4] S. Moncada, R.M.J. Palmer, E.A. Higgs, Pharmacol. Rev. 43 (1991) 109.
[5] C.L. Jenkins, Arch. Environ. Health 40 (5) (1978) 7.
[6] O. Yoshida, T. Harada, M. Miyagawa, T. Kato, Igaku No. Ayumi 79 (1971) 421.
[7] D.L. Jeffords, P.H. Lange, W.C. DeWolf, Urology 9 (1977) 180.
[8] K. Ikeda, Y. Sannohe, S. Araki, S. Inutsuka, Endoscopy 14 (4) (1982) 119.
[9] M. Vautier, C. Guillard, J.M. Hermann, J. Catal. 201 (2001) 46.
[10] C. Galindo, P. Jacques, A. Kalt, J. Photochem. Photobiol. A: Chem. 141 (2001) 47.
[11] A.H. Gemeay, I.A. Amsour, R.G. El-Sharkawy, A.B. Zaki, J. Photochem. Photobiol. A: Chem. 193 (2003) 109.
[12] C. Flox, S. Ammar, C. Arias, E. Brillas, A.V. Vargas-Zavala, R. Abdelhedi, Appl. Catal. B: Environ. 67 (2006) 93.
[13] A. Verberckmoes, B.M. Weckhuysen, R.A. Schoonheydt, Micropor. Mesopor. Mater. 22 (1998) 165.
[14] J.B. Yin, X.P. Zhou, Chem. Mater. 14 (2002) 4633.
[15] Y. Komoda, N. Sakai, T.N. Rao, Langmuir 14 (1998) 1081.
[16] R. Arroyo, G. Cordoba, J. Padilla, V.H. Lara, Mater. Lett. 54 (2002) 397.
[17] A.T. Stone, J.J. Morgan, Environ. Sci. Technol. 18 (1984) 617.
[18] W.G. Sunda, D.J. Kieber, Nature 367 (1994) 62.
[19] R. Liu, H. Tang, Water Res. 34 (2000) 4029.
[20] T.D. Waite, I. Wrgley, R. Szymczak, Environ. Sci. Technol. 22 (1988) 778.
[22] X.T. Yoko, K. Kamiya, K. Tanaka, J. Mater. Sci. 25 (1990) 3922.
[23] J. Zhang, I. Boyd, B.J.O. Sullivan, P.K. Hurley, P.V. Kelly, J.P. Senateur, J. Non-Cryst. Solid 303 (2002) 134.
[24] M.I. Zaki, M.A. Hasan, L. Pasupulety, K. Kumari, Thermochim. Acta 303 (1997) 171.
[25] F.A. Al-Sogheer, M.I. Zaki, Micropor. Mesopor. Mater. 67 (2004) 43.
[26] M.M. Mohamed, J. Colloid Interf. Sci. 272 (2004) 28.
[27] I. Othman, R.M. Mohamed, I.A. Ibrahim, M.M. Mohamed, Appl. Catal. A 299 (2006) 95.
[28] R.M. Potter, G.R. Rossman, Am. Miner. 64 (1979) 1199.
[29] A. Yamakata, T. Aki Ishibashi, H. Onishi, Bull. Chem. Soc. Jpn. 75 (2002) 1019.
[30] P. Jackson, G.D. Parfitt, Trans. Faraday Soc. 67 (1971) 2469.
[31] M. Primet, P. Pichat, M.-V. Mathieu, J. Phys. Chem. 75 (1971) 1216.
[32] A.T. Stone, Environ. Sci. Technol. 21 (1987) 979.
[33] P. Mulvaney, L. Denison, F. Grieser, R. Cooper, J.V. Sanders, D. Meisel, J. Colloid Interf. Sci. 121 (1988) 71.
[34] L. Canali, D.C. Sherrington, Chem. Soc. Rev. 28 (1999) 85.